Proton-beam stopping in hydrogen

J. J. Bailey, I. B. Abdurakhmanov, A. S. Kadyrov, I. Bray, and A. M. Mukhamedzhanov

Proton beam stopping in hydrogen

J. J. Bailey, I. B. Abdurakhmanov, A. S. Kadyrov, and I. Bray

Curtin Institute for Computation and Department of Physics and Astronomy,
Curtin University, GPO Box U1987, Perth, WA 6845, Australia

A. M. Mukhamedzhanov

Cyclotron Institute, Texas A&M University, College Station, Texas 77843, USA
(Dated: March 12, 2019)

The stopping cross section for protons passing through hydrogen is calculated for the energy range between 10 keV and 3 MeV. Both the positive and neutral charge-states of the projectile are accounted for. The two-centre convergent close-coupling method is used to model proton collisions with hydrogen. In this approach electron-capture channels are explicitly included by expanding the scattering wave function in a basis of both target and projectile pseudostates. Hydrogen collisions with hydrogen are modelled using two methods: the single-centre convergent close-coupling approach is used for the calculation of one-electron processes, while two-electron processes are calculated using the Born approximation. The aforementioned approaches are also applied to the calculation of the charge-state fractions. These are then used to combine the proton-hydrogen and hydrogen-hydrogen stopping cross sections to yield the total stopping cross section for protons passing through hydrogen.

PACS numbers: 34.10.+x, 34.50.Bw

I. INTRODUCTION

Any application of ion transport through matter is dependent on knowledge of energy losses during ion-atom collisions. Therefore, stopping power data are fundamentally important in a great number of fields, including medical radiation therapy [1, 2], aviation and space exploration [3], and astrophysics [4].

In this work we explore the topic of stopping powers from a theoretical perspective. Specifically, we will be focusing on the simplest target, being atomic hydrogen, and looking at how the stopping power of this atom is calculated for proton projectiles. When calculating the stopping power of hydrogen, energy losses due to electronic excitation and ionisation processes must be included. On top of this, collisions involving protons include the possibility for electron capture, in which the proton grabs the target electron forming a hydrogen atom. This process plays an important role in the calculation of the stopping power and, therefore, must also be included if one wishes to obtain accurate results. However, including electron-capture processes significantly increases the complexity of calculations as the problem requires a two-centre approach. Additionally, the electron-capture process in proton-hydrogen collisions further complicates the calculations as the newly formed hydrogen atom will continue interacting with the stopping medium. Therefore, when calculating the stopping power of hydrogen for protons one must also consider the collisions of hydrogen with hydrogen. Not only does the aforementioned collision system have a possibility of excitation and ionisation of the target, but now excitation and ionisation of the projectile is also possible. These processes can occur individually, resulting in single excitation or ionisation, or simultaneously, resulting in double excitation, double ionisation, or ionisation

with excitation. All these reaction channels must be included in the calculation of the stopping power. The total stopping power of hydrogen for protons then becomes the sum of the proton-hydrogen and hydrogen-hydrogen stopping powers weighted by their corresponding charge-state fractions. Here we present our approach to calculating the stopping power of hydrogen for protons and compare the results to the experimental data and theoretical calculations by other groups. There is currently no experimental data for proton stopping in atomic hydrogen. For this reason theoretical calculations are usually compared to experimental measurements involving a molecular hydrogen target. Measurements of the stopping cross section for protons passing through a H_2 gas, which cover the range from 10 keV to 2 MeV, have been performed by Reynolds *et al.* [5], Reiter *et al.* [6], and Golser and Semrad [7].

The first theoretical study of proton stopping in atomic hydrogen was performed by Dalgarno and Griffing [8]. They applied the first Born approximation (FBA) to calculate the proton-hydrogen and hydrogen-hydrogen stopping cross sections. Rearrangement processes in the case of proton-hydrogen scattering and two-electron processes in the case of hydrogen-hydrogen scattering were included. The results were combined by weighting each contribution by its charge-state fraction to obtain the total stopping cross section. Agreement with the experimental data for protons passing through H_2 was obtained above 120 keV, however their calculations underestimated the data at low energies. This discrepancy was attributed to the failure of the Bragg additivity rule in the proton-hydrogen fraction.

Schiwietz [9] performed single-centre coupled-channel atomic-orbital (AO) calculations for the proton fraction of the beam. They used the FBA calculations for the hydrogen fraction (including only single-excitation

and single-ionisation processes) and the experimental H_2 charge-state fractions of Allison [10] to obtain the total stopping cross section. Agreement with the calculations of Dalgarno and Griffing [8] above 125 keV was obtained. Also, agreement with experiment within 5% was achieved at low and high energies, however results underestimated the experiment by 10-15% at intermediate energies. It was suggested that the deterioration was due to an inaccurate ionisation cross section in hydrogen-hydrogen collisions as electron-electron correlations were neglected.

Schiwietz and Grande [11] further developed the aforementioned AO method of Schiwietz [9] by replacing the single-centre AO results below 30 keV with two-centre (AO+) ones, which included electron capture. The result was a significant reduction in the proton-hydrogen stopping cross section in this region. Additionally, a screened potential was used to perform AO calculations for hydrogen-hydrogen collisions, including only single excitation and single ionisation. Continuing to use the experimental H_2 charge-state fractions, these authors achieved 5% agreement with the H_2 stopping-power experiments over the whole energy range from 10 keV to 500 keV.

Fainstein *et al.* [12] used the continuum distorted-wave eikonal initial-state (CDW-EIS) method to calculate the stopping cross section for protons impinging on atomic hydrogen. When combined with the FBA hydrogen-hydrogen results of Dalgarno and Griffing [8] good agreement with experiment was obtained above 70 keV. Disagreement with the experiment below 70 keV was attributed to the usage of the FBA in the hydrogen-hydrogen channel. Agreement with all previous calculations was obtained above 125 keV, however, different results were obtained below this.

In this work the stopping cross sections corresponding to both the positive and neutral charge-states of the projectile are calculated and combined to yield the total stopping cross section for protons passing through hydrogen. To model proton-hydrogen collisions we use the two-centre convergent close-coupling (CCC) method. In this approach electron-capture channels are explicitly included by expanding the scattering wave function in a basis made of both target and projectile states. This is important for calculating both the stopping cross section and charge-state fractions. These calculations improve upon the work of Schiwietz and Grande [11] by employing a two-centre approach over the whole energy region considered as well as by including more target and projectile states in the expansion of the scattering wave function required for convergence. To model hydrogen-hydrogen collisions we use a combination of two approaches, the first is the single-centre CCC method and the second is the FBA. The usage of the single-centre approach is justified as the probability of H^- formation is very small. In the single-centre CCC approach one atom remains fixed in the ground state. Therefore, only single excitation and single ionisation can be taken into account, however

coupling between the channels is included. Subsequently, the first Born approximation is used to account for the two-electron processes of double excitation, double ionisation, and ionisation with excitation. These calculations improve upon those of Dalgarno and Griffing [8] by including excitations up to the $n = 8$ shell as opposed to $n = 3$.

We neglect electron exchange in the H-H channels as it was done in all the aforementioned calculations of the stopping power. The spin effects are expected to be small in the energy range between 10 keV and 3 MeV where we apply our method. However, at low energies, in particular around 10 keV and below, the spin effects become important [13–16]. Nevertheless, to our best knowledge, there has been no attempt to include them in stopping power calculations.

In addition to the non-exchange approximation mentioned above, we neglect electron transfer in H-H collisions. Thus the solution we present is not complete. Though we neglect electron transfer in H-H collisions, we do take into account total electron loss by one of the hydrogen atoms. In other words, we do not completely neglect electron transfer but take it into account implicitly (our approach cannot differentiate whether the lost electron has been captured by the other atom or not). As we will see later (see Sect. III B), comparison of the total cross section for electron loss in H-H collisions with experiment indicates that overall electron-loss processes have been modelled sufficiently accurately.

The single-centre CCC approach has previously been applied to the calculation of stopping cross sections for antiproton collisions with atoms and molecules [17–19] and to the calculation of scattering cross sections for antiproton-hydrogen collisions [20, 21]. Additionally, the two-centre CCC approach has been applied to the calculation of scattering cross sections for proton-hydrogen collisions [22–24]. Preliminary results of the proton-hydrogen stopping cross section using the two-centre CCC approach have been reported in Ref. [25].

The paper is set out as follows. Section II outlines the method. The results of calculations are presented and discussed in Sect. III. Finally, in Sect. IV we draw conclusions.

II. DESCRIPTION OF THE APPROACH

For CCC calculations we use the semiclassical approximation to formulate a set of coupled-channel differential equations that describe the scattering system. In the semiclassical approximation the target electron is treated fully quantum-mechanically while the motion of the projectile is treated classically. In the laboratory frame the projectile is assumed to be moving with velocity $\boldsymbol{v}$ along a straight line toward the target at an impact parameter $\boldsymbol{b}$. The position of the projectile with respect to the target nucleus is then given by $\boldsymbol{R}(t) = \boldsymbol{b} + \boldsymbol{v}t$, where t is time and $t = 0$ corresponds to the distance of closest

approach. The velocity of the projectile is taken to be along the z-axis and the impact parameter is taken to be along the x-axis. The position of the projectile along the z-axis is hence $z = vt$.

A. proton-hydrogen collisions

The two-centre CCC approach is based on the exact time-independent Schrödinger equation and uses an expansion for the total scattering wave function that correctly represents both the target and projectile centres. Here we describe the main steps. More details are given in Refs. [24, 26].

To describe the proton-hydrogen system we utilise the Jacobi coordinates where $\boldsymbol{r}_\mathrm{T}$ is the position of the electron relative to the target proton, while $\boldsymbol{r}_\mathrm{P}$ is the position of the electron relative to the projectile proton, and $\boldsymbol{\sigma}_\mathrm{T}$ is the position of the projectile proton relative to the centre-of-mass of the target proton-electron system, while $\boldsymbol{\sigma}_\mathrm{P}$ is the position of the centre-of-mass of the projectile proton-electron system relative to the target proton. Finally, $\boldsymbol{r}$ is the position of the electron relative to the centre-of-mass of the two-proton system.

The exact nonrelativistic Schrödinger equation for the total scattering wave function Ψ is written as

$$H\Psi = E\Psi, \tag{1}$$

where E is the total energy of the system and H is the full three-body Hamiltonian. The Hamiltonian can be written in the following equivalent forms:

$$H = -\frac{1}{2\mu}\nabla^2_{\boldsymbol{\sigma}_\mathrm{T}} + H_\mathrm{T} + V_\mathrm{P} = -\frac{1}{2\mu}\nabla^2_{\boldsymbol{\sigma}_\mathrm{P}} + H_\mathrm{P} + V_\mathrm{T}. \tag{2}$$

Here μ is the reduced mass of the proton-hydrogen system, H_T and H_P are the target and projectile atom Hamiltonians, V_T is the interaction of the target proton with the projectile atom, and V_P is the interaction of the projectile proton with the target atom. Hamiltonians H_T and H_P are given by

$$H_\mathrm{T} = -\frac{1}{2}\nabla^2_{\boldsymbol{r}_\mathrm{T}} - \frac{1}{r_\mathrm{T}}, \quad H_\mathrm{P} = -\frac{1}{2}\nabla^2_{\boldsymbol{r}_\mathrm{P}} - \frac{1}{r_\mathrm{P}}, \tag{3}$$

while the interactions V_T and V_P are given by

$$V_\mathrm{T} = \frac{1}{R} - \frac{1}{r_\mathrm{T}}, \quad V_\mathrm{P} = \frac{1}{R} - \frac{1}{r_\mathrm{P}}. \tag{4}$$

The total scattering wave function is expanded in terms of a set of N_T target pseudostates ψ_α and N_P projectile pseudostates ψ_β according to

$$\Psi = \sum_{\alpha=1}^{N_\mathrm{T}} A_\alpha(\boldsymbol{\sigma}_\mathrm{T})\psi_\alpha(\boldsymbol{r}_\mathrm{T})e^{i\boldsymbol{k}_\alpha\cdot\boldsymbol{\sigma}_\mathrm{T}}$$
$$+ \sum_{\beta=1}^{N_\mathrm{P}} B_\beta(\boldsymbol{\sigma}_\mathrm{P})\psi_\beta(\boldsymbol{r}_\mathrm{P})e^{i\boldsymbol{k}_\beta\cdot\boldsymbol{\sigma}_\mathrm{P}}, \tag{5}$$

where $\boldsymbol{k}_\alpha$ is the relative momentum of the projectile proton and the target atom in channel α, and similarly $\boldsymbol{k}_\beta$ is the relative momentum of the target proton and the projectile atom in channel β. The total energy of the system E is given by

$$E = \frac{k_\alpha^2}{2\mu} + \epsilon_\alpha = \frac{k_\beta^2}{2\mu} + \epsilon_\beta. \tag{6}$$

Furthermore, the pseudostates ψ_α and ψ_β represent both bound and continuum states, and are constructed to satisfy the conditions

$$\langle\psi_{\gamma'}|H_{\mathrm{T(P)}}|\psi_\gamma\rangle = \epsilon_\gamma\delta_{\gamma'\gamma}, \quad \langle\psi_{\gamma'}|\psi_\gamma\rangle = \delta_{\gamma'\gamma}. \tag{7}$$

It must be emphasised, that although the pseudostates within each set are orthogonal to each other, a pseudostate from one set is not orthogonal to a pseudostate from the other set. Details of the pseudostates are given in Sect. II C.

The scattering wave function (5) is substituted into the Schrödinger equation (1) and the result is projected onto to conjugate of each term in the expansion, i.e. $\psi_{\alpha'}^*(\boldsymbol{r}_\mathrm{T})e^{-i\boldsymbol{k}_{\alpha'}\cdot\boldsymbol{\sigma}_\mathrm{T}}$ and $\psi_{\beta'}^*(\boldsymbol{r}_\mathrm{P})e^{-i\boldsymbol{k}_{\beta'}\cdot\boldsymbol{\sigma}_\mathrm{P}}$. After applying the semiclassical approximation and some lengthy algebra we arrive at the final set of two-centre coupled-channel differential equations that describes proton scattering from hydrogen:

$$\begin{cases} i\dot{A}_{\alpha'} + i\sum_{\beta=1}^{N_\mathrm{P}}\dot{B}_\beta\mathcal{K}_{\alpha'\beta} = \sum_{\alpha=1}^{N_\mathrm{T}}A_\alpha\mathcal{D}_{\alpha'\alpha} + \sum_{\beta=1}^{N_\mathrm{P}}B_\beta\mathcal{Q}_{\alpha'\beta}, \\ i\sum_{\alpha=1}^{N_\mathrm{T}}\dot{A}_\alpha\tilde{\mathcal{K}}_{\beta'\alpha} + i\dot{B}_{\beta'} = \sum_{\alpha=1}^{N_\mathrm{T}}A_\alpha\tilde{\mathcal{Q}}_{\beta'\alpha} + \sum_{\beta=1}^{N_\mathrm{P}}B_\beta\tilde{\mathcal{D}}_{\beta'\beta}, \\ \alpha' = 1,\ldots,N_\mathrm{T}, \quad \beta' = 1,\ldots,N_\mathrm{P}, \end{cases} \tag{8}$$

where the dots over A and B denote the time derivative. In Eq. (8) the direct-scattering matrix elements $\mathcal{D}_{\alpha'\alpha}$ and $\tilde{\mathcal{D}}_{\beta'\beta}$ are given as

$$\mathcal{D}_{\alpha'\alpha} = e^{i(\epsilon_{\alpha'}-\epsilon_\alpha)t}\int d\boldsymbol{r}_\mathrm{T}\psi_{\alpha'}^*(\boldsymbol{r}_\mathrm{T})V_\mathrm{P}\psi_\alpha(\boldsymbol{r}_\mathrm{T}) \tag{9}$$

and

$$\tilde{\mathcal{D}}_{\beta'\beta} = e^{i(\epsilon_{\beta'}-\epsilon_\beta)t}\int d\boldsymbol{r}_\mathrm{P}\psi_{\beta'}^*(\boldsymbol{r}_\mathrm{P})V_\mathrm{T}\psi_\beta(\boldsymbol{r}_\mathrm{P}). \tag{10}$$

The overlap matrix elements $\mathcal{K}_{\alpha'\beta}$ and $\tilde{\mathcal{K}}_{\beta'\alpha}$ are

$$\mathcal{K}_{\alpha'\beta} = e^{i(-v^2t/2+(\epsilon_{\alpha'}-\epsilon_\beta)t)}\int d\boldsymbol{r}_\mathrm{T}\psi_{\alpha'}^*(\boldsymbol{r}_\mathrm{T})e^{i\boldsymbol{v}\cdot\boldsymbol{r}_\mathrm{T}}\psi_\beta(\boldsymbol{r}_\mathrm{P}) \tag{11}$$

and

$$\tilde{\mathcal{K}}_{\beta'\alpha} = e^{i(-v^2t/2+(\epsilon_{\beta'}-\epsilon_\alpha)t)}\int d\boldsymbol{r}_\mathrm{P}\psi_{\beta'}^*(\boldsymbol{r}_\mathrm{P})e^{-i\boldsymbol{v}\cdot\boldsymbol{r}_\mathrm{P}}\psi_\alpha(\boldsymbol{r}_\mathrm{T}), \tag{12}$$

and the electron-transfer matrix elements $\mathcal{Q}_{\alpha'\beta}$ and $\tilde{\mathcal{Q}}_{\beta'\alpha}$ are

$$
\begin{aligned}
\mathcal{Q}_{\alpha'\beta} = {} & e^{i(-v^2 t/2+(\epsilon_{\alpha'}-\epsilon_\beta)t)} \\
& \times \int d\boldsymbol{r}_{\mathrm{T}} \psi_{\alpha'}^*(\boldsymbol{r}_{\mathrm{T}}) e^{i\boldsymbol{v}\cdot\boldsymbol{r}_{\mathrm{T}}} (H_{\mathrm{P}} + V_{\mathrm{T}} - \epsilon_\beta) \psi_\beta(\boldsymbol{r}_{\mathrm{P}})
\end{aligned}
$$
(13)

and

$$
\begin{aligned}
\tilde{\mathcal{Q}}_{\beta'\alpha} = {} & e^{i(-v^2 t/2+(\epsilon_{\beta'}-\epsilon_\alpha)t)} \\
& \times \int d\boldsymbol{r}_{\mathrm{P}} \psi_{\beta'}^*(\boldsymbol{r}_{\mathrm{P}}) e^{-i\boldsymbol{v}\cdot\boldsymbol{r}_{\mathrm{P}}} (H_{\mathrm{T}} + V_{\mathrm{P}} - \epsilon_\alpha) \psi_\alpha(\boldsymbol{r}_{\mathrm{T}}).
\end{aligned}
$$
(14)

In Eqs. (8)-(14) the exponential factors arise naturally and not from the introduction of electron translation factors. For details see Refs. [24, 26].

The system of differential equations (8) is solved with the initial condition $A_{\alpha'}(t = -\infty, \boldsymbol{b}) = \delta_{\alpha' i}$ and $B_{\beta'}(t = -\infty, \boldsymbol{b}) = 0$. This implies the target is in the initial state ψ_i. For all calculations we take $i = 1s$, i.e. the target is initially in the ground state. The dependence of $A_{\alpha'}$ and $B_{\beta'}$ on the orientation of $\boldsymbol{b}$ can be factored such that the probability for transition from some initial state state of the target i into any final target state f or any final projectile state k is given by

$$
\begin{aligned}
p_f(b) &= |A_f(t = +\infty, b) - \delta_{fi}|^2, \\
p_k(b) &= |B_k(t = +\infty, b)|^2,
\end{aligned}
$$
(15)

where $A_f(t = +\infty, b)$ and $B_k(t = +\infty, b)$ are the probability amplitudes. The set of equations (8) is solved within the region $[-z_{\max}, z_{\max}]$, where parameter $z_{\max}$ is increased until convergent results are obtained. Direct-scattering matrix elements are evaluated in spherical coordinates, while overlap and electron-transfer matrix elements are evaluated in prolate spheroidal coordinates [22, 26].

B. hydrogen-hydrogen collisions

For the collisions of hydrogen with hydrogen we must introduce the coordinate $\boldsymbol{r}_{\mathrm{P}}'$, which is the position of the projectile electron relative to the projectile nucleus. As previously stated, we use a single-centre CCC approach for the calculation of one-electron processes and the first Born approximation for the calculation of two-electron processes (B2e). The details of both methods are given here. Together we refer to this as the "CCC+B2e" approach.

First, we consider the single-centre CCC approach. With the projectile atom fixed in the ground state the total scattering wave function is expanded in terms of a complete set of N_{T} target pseudostates ψ_α according to

$$
\Psi = \sum_{\alpha=1}^{N_{\mathrm{T}}} A_\alpha(\boldsymbol{\sigma}_{\mathrm{T}}) \psi_\alpha(\boldsymbol{r}_{\mathrm{T}}) \psi_{1s}(\boldsymbol{r}_{\mathrm{P}}') e^{i\boldsymbol{k}_\alpha \cdot \boldsymbol{\sigma}_{\mathrm{T}}}.
$$
(16)

Details of target pseudostates are given in Sect. II C. Additionally, the total energy of the system E is given by

$$
E = \frac{k_\alpha^2}{2\mu} + \epsilon_\alpha + \epsilon_{1s},
$$
(17)

and the total Hamiltonian H is written as

$$
H = -\frac{1}{2\mu}\nabla_{\boldsymbol{\sigma}_{\mathrm{T}}}^2 + H_{\mathrm{T}} + H_{\mathrm{P}}' + V_{\mathrm{P}},
$$
(18)

where μ is the reduced mass of the hydrogen-hydrogen system. Here H_{T} is the target atom Hamiltonian defined earlier in Eq. (3) and the projectile atom Hamiltonian H_{P}' is given by

$$
H_{\mathrm{P}}' = -\frac{1}{2}\nabla_{r_{\mathrm{P}}'}^2 - \frac{1}{r_{\mathrm{P}}'}.
$$
(19)

Also, V_{P} is the projectile-target interaction, which is given by

$$
V_{\mathrm{P}} = \frac{1}{R} - \frac{1}{|\boldsymbol{R} - \boldsymbol{r}_{\mathrm{T}}|} - \frac{1}{|\boldsymbol{R} + \boldsymbol{r}_{\mathrm{P}}'|} + \frac{1}{|\boldsymbol{R} + \boldsymbol{r}_{\mathrm{P}}' - \boldsymbol{r}_{\mathrm{T}}|}.
$$
(20)

Substituting the scattering wave function (16) into the Schrödinger equation (1) and following the same procedure as in Section II A we obtain the final set of coupled-channel differential equations

$$
i\dot{A}_{\alpha'} = \sum_{\alpha=1}^{N_{\mathrm{T}}} A_\alpha \mathcal{H}_{\alpha'\alpha}; \ \alpha' = 1, \dots, N_{\mathrm{T}},
$$
(21)

where $\mathcal{H}_{\alpha'\alpha}$ are the direct-scattering matrix elements

$$
\begin{aligned}
\mathcal{H}_{\alpha'\alpha} = {} & e^{i(\epsilon_{\alpha'}-\epsilon_\alpha)t} \\
& \times \int d\boldsymbol{r}_{\mathrm{T}} d\boldsymbol{r}_{\mathrm{P}}' \psi_{\alpha'}^*(\boldsymbol{r}_{\mathrm{T}}) \psi_{1s}(\boldsymbol{r}_{\mathrm{P}}') V_{\mathrm{P}} \psi_{1s}(\boldsymbol{r}_{\mathrm{P}}') \psi_\alpha(\boldsymbol{r}_{\mathrm{T}}).
\end{aligned}
$$
(22)

Equation (21) is solved in a similar manner described for the proton-hydrogen system.

To model two-electron processes, i.e. double excitation, double ionisation, and ionisation with excitation we use the FBA. In the Born approximation the transition amplitude for the scattering process $\mathrm{H}(1s) + \mathrm{H}(1s) \to \mathrm{H}(\alpha) + \mathrm{H}(\beta)$ is given by

$$
\begin{aligned}
T_{\alpha,\beta} = {} & \iiint d\boldsymbol{r}_{\mathrm{T}} d\boldsymbol{r}_{\mathrm{P}}' d\boldsymbol{R}\, \psi_{1s}(\boldsymbol{r}_{\mathrm{T}}) \psi_\alpha^*(\boldsymbol{r}_{\mathrm{T}}) \psi_{1s}(\boldsymbol{r}_{\mathrm{P}}') \psi_\beta^*(\boldsymbol{r}_{\mathrm{P}}') \\
& \times e^{i\boldsymbol{K}\cdot\boldsymbol{R}} \left(\frac{1}{R} - \frac{1}{|\boldsymbol{R} + \boldsymbol{r}_{\mathrm{P}}'|} - \frac{1}{|\boldsymbol{R} - \boldsymbol{r}_{\mathrm{T}}|} \right. \\
& \left. + \frac{1}{|\boldsymbol{R} + \boldsymbol{r}_{\mathrm{P}}' - \boldsymbol{r}_{\mathrm{T}}|} \right).
\end{aligned}
$$
(23)

Here $\boldsymbol{K} = \boldsymbol{k}_i - \boldsymbol{k}_f$ is the momentum transfer, where $\boldsymbol{k}_i$ and $\boldsymbol{k}_f$ are the initial and final momenta of the projectile, respectively. For FBA calculations we will choose $\boldsymbol{K}$ to be along the z-axis. Additionally, α and β represent

the final states of the target and projectile atoms, respectively. If the final state of the target is a bound state then $\alpha = n_\alpha l_\alpha m_\alpha$, where n, l, and m are the principal, orbital, and magnetic quantum numbers, and $\psi_\alpha = \psi_{n_\alpha l_\alpha m_\alpha}$ is the eigenstate wave function of the hydrogen atom. On the other-hand, if the final state of the target is a continuum state then we use the momentum of the ejected electron $\boldsymbol{k}_e$ as the channel index, i.e. $\alpha = \boldsymbol{k}_e$, and $\psi_\alpha = \psi_{\boldsymbol{k}_e}^-$ is the two-body Coulomb wave function (see below). Similarly, if the final state of the projectile is a bound state then $\beta = n_\beta l_\beta m_\beta$, and if it is a continuum state then $\beta = \boldsymbol{k}_e'$.

Equation (23) can be evaluated analytically to get

$$T_{\alpha,\beta} = \frac{4\pi}{K^2}\big(\delta_{\alpha,1s} - \mathcal{F}_\alpha(\boldsymbol{K})\big)\big(\delta_{\beta,1s} - \mathcal{F}_\beta(-\boldsymbol{K})\big), \quad (24)$$

where

$$\mathcal{F}_\gamma(\boldsymbol{K}) = \int d\boldsymbol{r}\,\psi_{1s}(\boldsymbol{r})\psi_\gamma^*(\boldsymbol{r})e^{i\boldsymbol{K}\cdot\boldsymbol{r}}. \quad (25)$$

The latter can be evaluated for any excitation transition. Since we choose $\boldsymbol{K}$ to be aligned along the z-axis the resulting amplitudes are non-zero only when the change in magnetic quantum number is equal to zero. As both atoms are initially in the ground state, only final states with $m = 0$ need to be considered and the amplitude becomes

$$\mathcal{F}_{nl}(K) = i^l\sqrt{2l+1}\int_0^\infty r^2 dr\,R_{10}(r)R_{nl}(r)j_l(Kr), \quad (26)$$

where R_{nl} are the radial functions and j_l is the spherical Bessel function of the first kind. Eq. (26) is evaluated analytically for a specific R_{nl}.

For ionisation transitions the final-state wave function is taken to be two-body Coulomb wave function. Following the ideas of Guth and Mullin [27] who calculated the Fourier transform of the Coulomb wave function, it can be shown that $\mathcal{F}_{\boldsymbol{k}_e}$ is given by

$$\mathcal{F}_{\boldsymbol{k}_e}(\boldsymbol{K}) = \frac{2\sqrt{2}}{\pi}e^{-\pi\eta/2}\Gamma(1+i\eta)\frac{\big[K^2 - (k_e + i)^2\big]^{i\eta}}{\big[(\boldsymbol{k}_e + \boldsymbol{K})^2 + 1\big]^{1+i\eta}}$$
$$\times\left(\frac{(1+i\eta)}{[(\boldsymbol{k}_e + \boldsymbol{K})^2 + 1]} + \frac{(1-i\eta)}{[K^2 - (k_e + i)^2]}\right), \quad (27)$$

where Γ is the Gamma function and $\eta = -1/k_e$ is the Sommerfeld parameter.

C. Target structure

The atomic hydrogen pseudostates used in CCC calculations are generated by following the ideas of Bray and Stelbovics [28]. The radial parts of the pseudostates ψ_α in Eqs. (5) and (16) are written as

$$R_{nl}(r) = \frac{1}{r}\sum_{k=1}^{N_l} B_{nk}^l \xi_{kl}(r), \quad (28)$$

where ξ_{kl} is a complete set of orthonormal basis functions, N_l is the number of basis functions for a given l, and B_{nk}^l are the expansion coefficients that are found by diagonalisation of the target Hamiltonian in the complete basis. In other words, the pseudostates ψ_α satisfy the conditions specified in Eq. (7).

In Eq. (28), we choose the basis functions to be the Laguerre functions

$$\xi_{kl}(r) = \left(\frac{\lambda_l(k-1)!}{(2l+1+k)!}\right)^{1/2}(\lambda_l r)^{l+1}$$
$$\times \exp(-\lambda_l r/2)L_{k-1}^{2l+2}(\lambda_l r), \quad (29)$$

where $L_{k-1}^{2l+2}(\lambda_l r)$ are the associated Laguerre polynomials and λ_l is an exponential fall-off parameter. Choice of λ_l does not affect the final result, however it does affect the speed of convergence. Specific values of λ_l will be given in Sect. III. The choice of the basis as a set of orthogonal Laguerre functions allows us to model the whole spectrum of the target atom. As the size of the one-electron basis increases the low-lying states will converge to the true bound states of the target, while the remaining negative-energy (pseudo) states will provide an effective representation of the high-lying bound states of the target atom. The positive-energy pseudostates provide and an increasingly dense square-integrable representation of the target continuum.

D. Stopping power

The stopping power is the energy loss per unit path length and is defined as

$$-\frac{dE}{dx} = N_a S(E_0), \quad (30)$$

where $S(E_0)$ is referred to as the stopping cross section. It depends on the incident energy of the projectile E_0, and is related to the stopping power through the density of target atoms in the stopping medium N_a. For heavy projectiles it can be assumed that the total stopping cross section is the sum of two contributions, the nuclear and the electronic stopping cross sections, i.e. $S = S_e + S_n$. In this work we consider only the electronic part of the stopping cross section as we are interested in incident energies above 10 keV where the nuclear part is insignificant. However, if one is interested in incident energies below 10 keV, calculation of the nuclear part is straightforward and is detailed in Ref. [18].

Due to the possibility of electron-capture the incident proton can grab the electron and form a hydrogen atom. This newly formed hydrogen atom will continue interacting with the stopping medium, losing energy and potentially losing and gaining electrons many times. For this reason all possible charge-states of the beam must be considered when calculating the total stopping cross section for protons incident on atomic hydrogen. The total stopping cross section for the proton-hydrogen system

is therefore given by

$$S(E_0) = f^{\mathrm{H}^+} S^{\mathrm{H}^+} + f^{\mathrm{H}^0} S^{\mathrm{H}^0}, \tag{31}$$

where S^{H^+} is the stopping cross sections for a beam consisting entirely of protons (positive charge), S^{H^0} is the stopping cross sections for a beam consisting entirely of hydrogen atoms (neutral charge), and f^{H^+} and f^{H^0} are the positive and neutral charge-state fractions of the beam, respectively. In this work we neglect the negative charge state as the probability of H^- formation is insignificant. The charge-state fractions f^{H^+} and f^{H^0} are calculated from the total electron-capture (EC) cross section σ_{EC} in proton-hydrogen collisions and the total electron-loss (EL) cross section σ_{EL} in hydrogen-hydrogen collisions according to

$$f^{\mathrm{H}^+} = \sigma_{\mathrm{EL}}/(\sigma_{\mathrm{EC}} + \sigma_{\mathrm{EL}}), \quad f^{\mathrm{H}^0} = \sigma_{\mathrm{EC}}/(\sigma_{\mathrm{EC}} + \sigma_{\mathrm{EL}}). \tag{32}$$

This highlights the importance of having a two-centre approach that can provide accurate electron-capture cross sections. Further details on σ_{EC} and σ_{EL} are given below.

The positive-charge-state electronic stopping cross section $S_{\mathrm{e}}^{\mathrm{H}^+}$ is the result of three possible energy-loss processes in the proton-hydrogen collision system. These are excitation and ionisation of the target, and capture of the target electron to a bound state of the projectile. The stopping cross section is therefore written as

$$S_{\mathrm{e}}^{\mathrm{H}^+} = \sum_{f=1}^{\infty} (\epsilon_f - \epsilon_i)\sigma_{fi} + \int_0^{E_0 + \epsilon_i} (\epsilon - \epsilon_i)\frac{d\sigma}{d\epsilon}d\epsilon \\ + \sum_{k=1}^{\infty} (\epsilon_k - \epsilon_i + v^2/2)\sigma_{ki}, \tag{33}$$

where ϵ_i is the energy of the ground state of the target i, σ_{fi} is the cross section for excitation to a state f of energy ϵ_f, $d\sigma/d\epsilon$ is the single differential cross section for ionisation when the electron is ejected with energy ϵ, and σ_{ki} is the cross section for electron capture to a state k of energy ϵ_k. Additionally, the $v^2/2$ term represents the kinetic energy of an electron travelling with the speed of the incident proton after being captured.

To accurately model electron-capture processes we use a two-centre coupled-channel approach with pseudostates centred on both the target and projectile, as described in Sect. II A. For the calculation of the stopping cross section we include bound and continuum pseudostates on the target centre, while only negative-energy pseudostates for the projectile centre. This is due to ambiguities in the calculation of the stopping power associated with electron capture into continuum process. Such issues have been explored in Ref. [24]. With this model the first two terms in Eq. (33) that represent excitation and ionisation become a single sum over N_{T} negative- and positive-energy target-centred pseudostates, while the third term becomes a sum over N_{P} negative-energy

projectile-centred pseudostates. Thus we obtain

$$S_{\mathrm{e}}^{\mathrm{H}^+} \approx \sum_{f=1}^{N_{\mathrm{T}}} (\epsilon_f - \epsilon_i)\sigma_{fi} + \sum_{k=1}^{N_{\mathrm{P}}} (\epsilon_k - \epsilon_i + v^2/2)\sigma_{ki}. \tag{34}$$

Here the cross sections for the direct transitions σ_{fi} and rearrangement transitions σ_{ki} are obtained by integration of the transition probabilities (15) over the impact parameter according to

$$\sigma_{fi} = 2\pi \int_0^{\infty} p_{fi}(b)b\,db, \quad \sigma_{ki} = 2\pi \int_0^{\infty} p_{ki}(b)b\,db. \tag{35}$$

Furthermore, the total electron-capture cross section σ_{EC}, which is required for the calculation of the charge-state fractions (32), is the sum of all electron-capture cross sections (35), i.e.

$$\sigma_{\mathrm{EC}} = \sum_{k=1}^{N_{\mathrm{P}}} \sigma_{ki}. \tag{36}$$

The neutral-charge-state electronic stopping cross section $S_{\mathrm{e}}^{\mathrm{H}^0}$ is the result of many possible energy-loss processes in the hydrogen-hydrogen collision system. These are excitation or ionisation of either the target or projectile, simultaneous excitation or ionisation of both the target and projectile, and excitation of either the target or projectile with ionisation of the other. Including all these terms the stopping cross section is written as

$$S_{\mathrm{e}}^{\mathrm{H}^0} = 2\sum_{f=1}^{\infty} (\epsilon_f - \epsilon_i)\sigma_{fi} + 2\int_0^{E_0 + \epsilon_i} (\epsilon - \epsilon_i)\frac{d\sigma}{d\epsilon}d\epsilon \\ + \sum_{f \neq i}^{\infty}\sum_{k \neq i}^{\infty} (\epsilon_f - \epsilon_i + \epsilon_k - \epsilon_i)\sigma_{fi,ki} \\ + \int_0^{E_0 + \epsilon_i}\int_0^{E_0 + \epsilon_i} (\epsilon - \epsilon_i + \epsilon' - \epsilon_i)\frac{d\sigma}{d\epsilon d\epsilon'}d\epsilon d\epsilon' \\ + 2\sum_{f \neq i}^{\infty}\int_0^{E_0 + \epsilon_i} (\epsilon_f - \epsilon_i + \epsilon - \epsilon_i)\frac{d\sigma_{fi}}{d\epsilon}d\epsilon, \tag{37}$$

where σ_{fi} is now the cross section for excitation of one hydrogen atom to a state f of energy ϵ_f while the other remains in the ground state, $d\sigma/d\epsilon$ is the differential cross section for ionisation of one hydrogen atom when the electron is ejected with energy ϵ while the other remains in the ground state, $\sigma_{fi,ki}$ is the cross section for excitation of both hydrogen atoms, one to a state f of energy ϵ_f and the other to a state k of energy ϵ_k, $d\sigma/d\epsilon d\epsilon'$ is the differential cross section for ionisation of both hydrogen atoms, one with energy ϵ and the other with energy ϵ', and $d\sigma_{fi}/d\epsilon$ is the differential cross section for ionisation of one hydrogen atom when the electron is ejected with energy ϵ while the other is excited to a state f of energy ϵ_f. Additionally, the factor of 2 in the first, third, and last terms of Eq. (37) is due to the symmetry of the system.

To model one-electron processes we use a single-centre coupled-channel approach. Since the continuum is discretised in this approach, the first and third terms of Eq. (37), which represent the stopping cross sections associated with single excitation and ionisation, become a single sum over N_T negative- and positive-energy pseudostates. To model two-electron processes we use the first Born approximation. In this approach we limit ourselves to a total of N_b bound states. Combining these two models the neutral-charge-state electronic stopping cross section (37) becomes

$$
\begin{aligned}
S_e^{H^0} =& 2\sum_{f=1}^{N_T}(\epsilon_f - \epsilon_i)\sigma_{fi} + \sum_{f\neq i}^{N_b}\sum_{k\neq i}^{N_b}(\epsilon_f - \epsilon_i + \epsilon_k - \epsilon_i)\sigma_{fi,ki} \\
&+ \int_0^{E_0+\epsilon_i}\int_0^{E_0+\epsilon_i}(\epsilon - \epsilon_i + \epsilon' - \epsilon_i)\frac{d\sigma}{d\epsilon d\epsilon'}d\epsilon d\epsilon' \\
&+ 2\sum_{f\neq i}^{N_b}\int_0^{E_0+\epsilon_i}(\epsilon_f - \epsilon_i + \epsilon - \epsilon_i)\frac{d\sigma_{fi}}{d\epsilon}d\epsilon,
\end{aligned} \tag{38}
$$

Here the cross sections for one-electron transitions σ_{fi} are obtained using Eq. (35). Additionally, the cross sections for the two-electron processes of double excitation, double ionisation, and ionisation with excitation are calculated from the Born transition amplitudes (24) according to

$$
\sigma_{fi,ki} = \frac{\mu^2}{2\pi k_i^2}\int |T_{n_f l_f, n_k l_k}|^2 K dK, \tag{39}
$$

$$
\frac{d\sigma}{d\epsilon d\epsilon'} = k_e k_e'\frac{\mu^2}{2\pi k_i^2}\iiint |T_{\boldsymbol{k}_e, \boldsymbol{k}_e'}|^2 K dK d\Omega_{\boldsymbol{k}_e}\Omega_{\boldsymbol{k}_e'}, \tag{40}
$$

and

$$
\frac{d\sigma_{fi}}{d\epsilon} = k_e\frac{\mu^2}{2\pi k_i^2}\iint |T_{n_f l_f, \boldsymbol{k}_e}|^2 K dK d\Omega_{\boldsymbol{k}_e}, \tag{41}
$$

respectively. In Eqs. (39)-(41), the integrals over K are over the range from $K_{\min} = k_i - k_f$ to $K_{\max} = k_i + k_f$ and evaluated numerically, while the integrals over $\Omega_{\boldsymbol{k}_e}$ are evaluated analytically. The final momentum of the projectile k_f is obtained from the energy-conservation law and depends on the final states of the atoms, while $\boldsymbol{k}_e$ is the momentum of the ejected electron. Furthermore, the total electron-loss cross section σ_{EL}, which is required for the calculation of the charge-state fractions (32), is the sum of all cross sections corresponding to ionisation of the target atom. Therefore, it is written as the sum of the total single-ionisation (SI) cross section σ_{SI}, total double-ionisation (DI) cross section σ_{DI}, and total ionisation-with-excitation (IE) cross section σ_{IE}, that is

$$
\sigma_{EL} = \sigma_{SI} + \sigma_{DI} + \sigma_{IE}. \tag{42}
$$

In the aforementioned model the total single-ionisation cross section is given by the sum of all cross sections for

one-electron transitions to positive-energy states:

$$
\sigma_{SI} = \sum_{f:\epsilon_f>0}^{N_T}\sigma_{fi}. \tag{43}
$$

The total double-ionisation and ionisation-with-excitation cross sections are calculated from Eqs. (40) and (41), respectively, as

$$
\sigma_{DI} = \int_0^{E_0+\epsilon_{1s}}\int_0^{E_0+\epsilon_{1s}}\frac{d\sigma}{d\epsilon d\epsilon'}d\epsilon d\epsilon', \tag{44}
$$

and

$$
\sigma_{IE} = \sum_{f\neq i}^{N_b}\int_0^{E_0+\epsilon_{1s}}\frac{d\sigma_{fi}}{d\epsilon}d\epsilon. \tag{45}
$$

III. RESULTS

In this section the results of our calculations for the proton-hydrogen electronic stopping cross section will be presented and compared to existing theoretical and experimental results. When using a coupled-channel approach where the scattering wave function is expanded in a set of target- and projectile-centered pseudostates it is important to establish convergence of the stopping cross section with increasing the size of the underlying basis. Therefore, we will start by specifying the basis parameters N_l and $l_{\max}$, where N_l is the number of basis functions for a given l and $l_{\max}$ is the maximum value of orbital angular momentum included in the expansion of the scattering wave function that produced the convergent result. Specifically, we say that convergence is achieved when the stopping cross section varies no more than 2% with an increase in either N_l or $l_{\max}$. Therefore, our calculations are estimated to be accurate to within 2%.

A. Proton-hydrogen stopping cross section

Convergence in calculations of the electronic stopping cross section for proton-hydrogen collisions was achieved with $l_{\max} = 8$ and $N_l = 30 - l$. These basis parameters result in a total of 1896 target states and 159 projectile states to be used in the solution of the coupled-channel differential equations (8). Also, the basis function exponential fall-off parameter λ_l is chosen to be 2 for all l.

In Fig. 1 we present our result for the proton-hydrogen electronic stopping cross section (SCS) together with the calculations of Dalgarno and Griffing [8], Schiwietz [9], Schiwietz and Grande [11], and Fainstein et al. [12]. We use the two-centre CCC approach, meaning energy losses due to electron-capture processes are explicitly included, as well as energy losses due to excitation and ionisation.
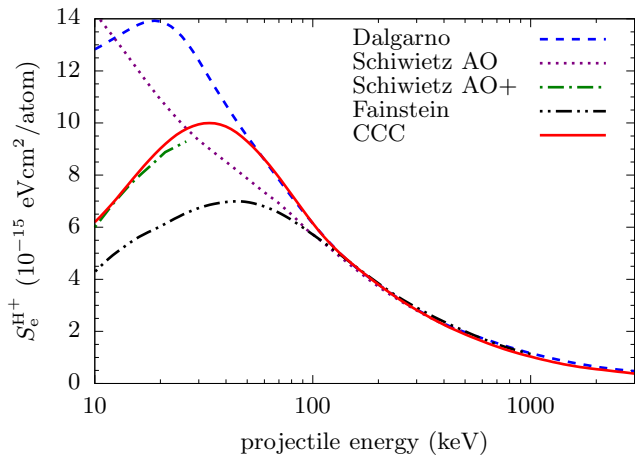
FIG. 1. Electronic stopping cross section for protons incident on hydrogen. The two-centre CCC calculations are compared with the results of Dalgarno and Griffing [8], Schiwietz [9] (AO), Schiwietz and Grande [11] (AO+), and Fainstein *et al.* [12].

FIG. 2. Individual contributions to the proton-hydrogen electronic stopping cross section. The curves labelled "Excitation" and "Ionisation" are the stopping cross sections associated with excitation and ionisation of the target atom, respectively. The curve labelled "Electron capture" represents the stopping cross section associated with electron capture.

The CCC results are in good agreement with the FBA calculation of Dalgarno and Griffing [8] above 50 keV. They are also in good agreement with the AO calculations of Schiwietz [9] and the CDW-EIS calculations of Fainstein *et al.* [12] above 130 keV. Furthermore, in the lower energy region we obtain reasonable agreement with the two-centre AO+ calculations of Schiwietz and Grande [11]. The fact that the CCC results are slightly higher than the AO+ ones above 15 keV is likely to be due to the inclusion of more target and projectile states in our calculations compared to those of Schiwietz and Grande [11]. In addition, comparing the single-centre AO calculations of Schiwietz [9] to the two-centre CCC and AO+ calculations we see that the explicit inclusion of electron-capture channels results in a significant difference in the proton-hydrogen electronic stopping cross section below 100 keV.

Individual contributions to the stopping cross section are presented in Fig. 2. This figure demonstrates that below 35 keV energy loss due to momentum transfer to the electron during electron capture is the dominant contribution to the stopping cross section, whereas above 35 keV the dominant contribution is due to ionisation. Additionally, it shows that energy losses associated with excitation of the target make a substantial contribution over the whole energy region, while electron-capture processes make a significant contribution only below 60 keV.

B. Hydrogen-hydrogen stopping cross section

Convergence in the CCC calculations of the electronic stopping cross section for hydrogen-hydrogen collisions was achieved with $l_{max} = 15$ and $N_l = 30 - l$. These basis parameters result in a total of 5080 target states
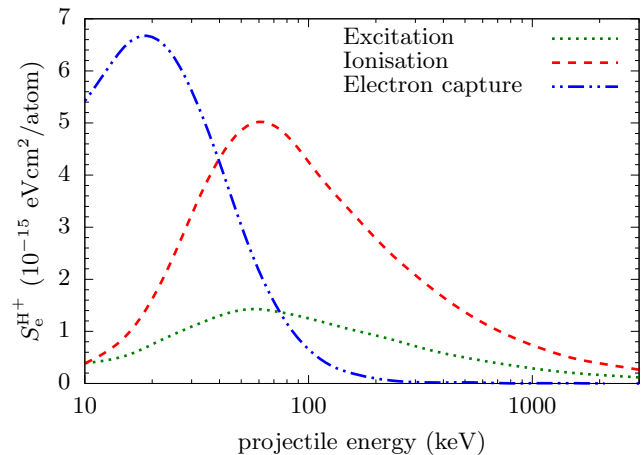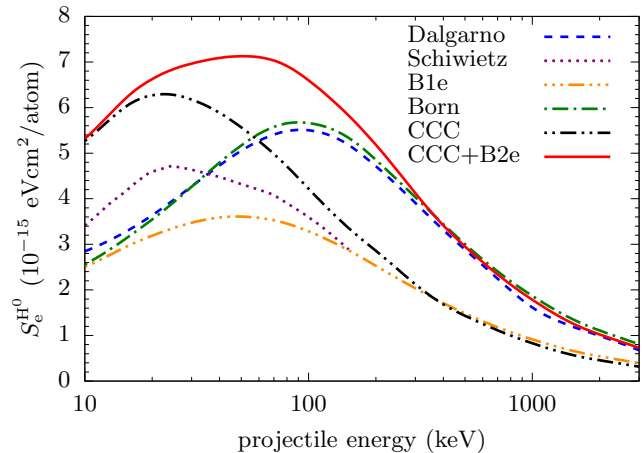

FIG. 3. Electronic stopping cross section for hydrogen incident on hydrogen. Calculations are compared with those of Dalgarno and Griffing [8], and Schiwietz and Grande [11]. The results labelled as "CCC" and "B1e" include one-electron processes only, while "CCC+B2e" and "Born" results include one- and two-electron processes (see text for details).

used in the solution of the coupled-channel differential equations (21). Also, the basis function exponential fall-off parameter λ_l is chosen to be 4 for all l. It should be noted that the value for l_{max} is significantly larger than that required for proton-hydrogen collisions due to the single-centre approach being used. This is to generate higher-energy continuum states compared to the proton calculations. Furthermore, in the Born calculations we include excitations to all states for which $n \leq 8$ and $l \leq 3$.

In Fig. 3 we present our CCC+B2e results for the hydrogen-hydrogen electronic stopping cross section to-

gether with the calculations of Dalgarno and Griffing [8], and Schiwietz and Grande [11]. The CCC+B2e calculations include energy losses due to single excitation and single ionisation that are calculated in the single-centre CCC approach, as well as energy losses due to double excitation, double ionisation, and ionisation with excitation that are calculated in the FBA. Also shown in Fig. 3 are the results arising solely from CCC calculations, meaning only energy losses due to single excitation and ionisation are included, as well as the results of the Born calculations for all energy loss processes (labelled as Born) and one-electron processes only (labelled as B1e). First, we note that the CCC results are in agreement with the B1e results at high energies where the latter is considered accurate. Specifically, good agreement is seen above 300 keV. However, at lower energies, below 200 keV, the coupling between channels in the CCC approach results in a significantly larger stopping cross section when compared to the B1e results. In this energy region CCC calculations are much larger than the AO calculations of Schiwietz and Grande [11] as well, although both methods are based on a somewhat similar approach. It could be that the results of Schiwietz and Grande [11] did not have a sufficient number of states as the CCC calculations include a much larger number of target states. Turning to the Born results we see a small but systematic disagreement with the FBA calculations of Dalgarno and Griffing [8] above 40 keV. This is due to the fact that we include excitation to all states with $n \leq 8$ and $l \leq 3$, whereas Dalgarno and Griffing [8] include excitations up to the $n = 3$ shell only. This fact has been verified by performing calculations that include the same number of states as Dalgarno and Griffing [8]. On the other hand, below 20 keV the FBA calculations of Dalgarno and Griffing [8] are slightly higher as they have included an estimated contribution to the stopping cross section due to H^- formation. Lastly, comparing our calculations that include one-electron processes (i.e. CCC and B1e) to those that include one- and two-electron processes (CCC+B2e and Born) we conclude that double excitation, double ionisation, and ionisation with excitation make a substantial contribution to the stopping cross section above 20 keV (further evidence for this conclusion is given in the next paragraph). As such, the CCC+B2e calculation is considered our most accurate result.

The conclusion drawn above can be validated by considering the total cross section for electron loss by the projectile as there is experimental data to compare with. Since the stopping cross section is dominated by ionisation processes (as shown below), this may prove useful in assessing the accuracy of the hydrogen-hydrogen stopping cross section. In Fig. 4 we present our CCC+B2e calculation for the total electron-loss cross section compared to the experimental data of Wittkower et al. [29] and McClure [30]. Also shown are the Born calculations for the total electron-loss cross section (Born EL), as well as the Born and single-centre CCC calculations for the single-ionisation cross section (denoted as Born SI and
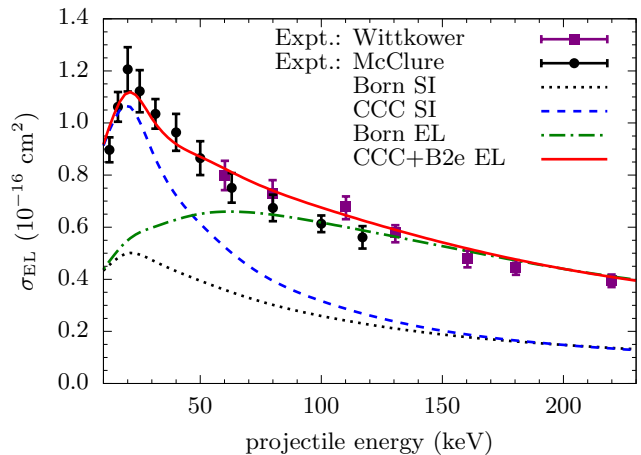

FIG. 4. Projectile total electron-loss cross section in hydrogen collisions with hydrogen. The CCC+B2e calculations (see text for details) are compared to the experimental data of Wittkower et al. [29] and McClure [30]. Also shown are the Born calculations for total electron loss (Born EL), as well as the Born and CCC calculations for single ionisation only, labelled "Born SI" and "CCC SI", respectively.

CCC SI, respectively). The CCC+B2e results are in good agreement with the experimental data over the whole energy region considered. On the other hand, the Born EL calculations significantly underestimate experiment below 70 keV projectile energy. This illustrates the benefit of using a coupled-channel approach for the one-electron processes, as is done presently. This becomes evident when we compare the CCC SI and Born SI calculations, where the latter significantly underestimates the former below 100 keV. Furthermore, the importance of including the two-electron processes becomes apparent when two models that include one-electron processes only, i.e. CCC SI and Born SI, are compared to those that include both one- and two-electron processes, i.e. CCC+B2e EL and Born EL. As can been seen, the CCC SI calculations underestimate experiment above 20 keV projectile energy and the Born SI calculations underestimate experiment at all projectile energies considered.

Individual contributions to the Born stopping cross section are presented in Fig. 5. This figure demonstrates that at high incident energies the stopping cross section is dominated by single- and double-ionisation processes, each making an almost equal contribution. In the intermediate energy region, energy losses due to single ionisation are the main contribution to the stopping cross section, while double ionisation and ionisation with excitation make a smaller but still significant addition. Double excitation also makes relatively small but important contribution in this region. Lastly, at lower incident energies the contribution from single-excitation processes increases and becomes significant, however, single ionisation remains dominant.

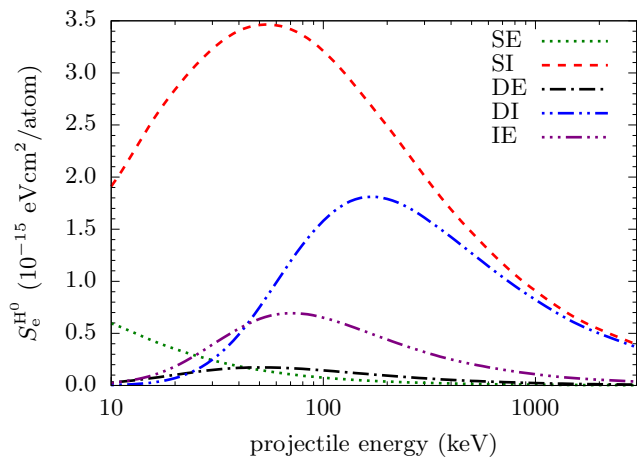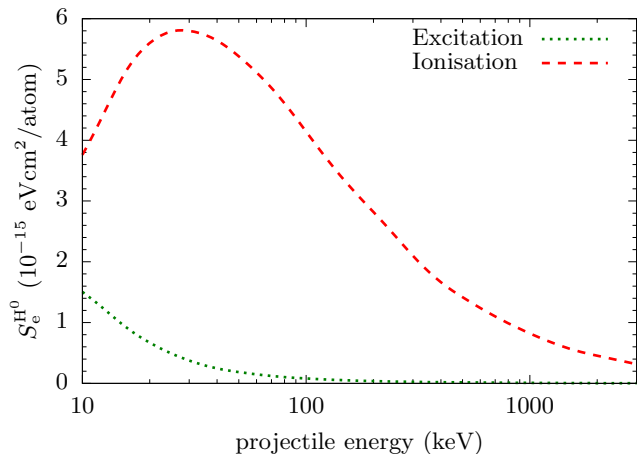The same but for the CCC stopping cross section are

FIG. 5. Individual contributions to the hydrogen-hydrogen electronic stopping cross section calculated in the Born approximation. The curves labelled "SE" and "SI" are the stopping cross sections associated with single excitation and ionisation, respectively. While the curves labelled "DE" and "DI" are the stopping cross sections associated with double excitation and double ionisation, respectively. Also, "IE" is the stopping cross section due to ionisation with excitation.

presented in Fig. 6. The figure shows that energy losses due to ionisation dominate the stopping cross section at all incident energies considered, while energy losses due to excitation make a significant contribution only below 50 keV.

FIG. 6. Individual contributions to the hydrogen-hydrogen electronic stopping cross section calculated with the CCC method. The curves labelled "Excitaiton" and "Ionisation" are the stopping cross sections associated with single excitation and single ionisation, respectively.
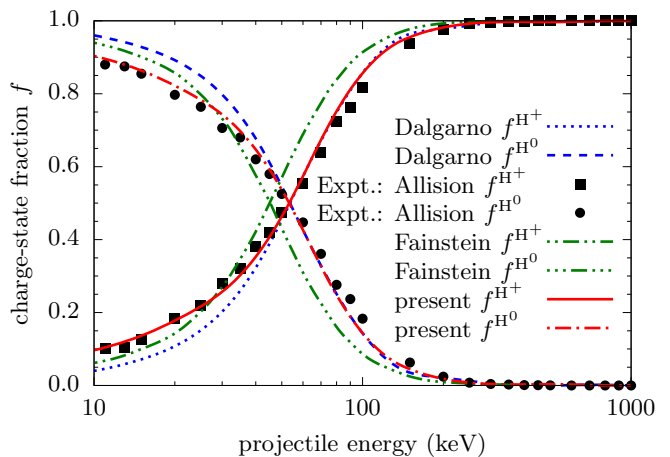

FIG. 7. Positive (f^{H^+}) and neutral (f^{H^0}) charge-state fractions for protons passing through hydrogen. The present results are compared to those of Dalgarno and Griffing [8], and Fainstein et al. [12]. The experimental data of Allison [10], which were measured for a molecular hydrogen target, are also shown.

C. Total stopping cross section

As discussed previously, the total stopping cross section for protons passing through hydrogen is calculated by summing the proton-hydrogen and hydrogen-hydrogen stopping cross sections weighted by their respective charge-state fractions. We remind that for the hydrogen-hydrogen stopping cross section we use the CCC+B2e result. Subsequently, the hydrogen-hydrogen total electron-loss cross section, which is required for the calculation of charge-state fractions, is the sum of the single-ionisation cross that is calculated in the single-centre CCC approach and the double-ionisation and ionisation-with-excitation cross sections that are calculated using the Born approximation.

In Fig. 7 we present our results for the positive (f^{H^+}) and neutral (f^{H^0}) charge-state fractions for a beam of protons passing through hydrogen. They are displayed alongside the calculations of Dalgarno and Griffing [8] and Fainstein et al. [12], as well as the experimental data of Allison [10] (which was used in the calculation of the total stopping cross section by Schiwietz [9] and Schiwietz and Grande [11]). We obtain good agreement with Dalgarno and Griffing [8] above 40 keV projectile energy and with Fainstein et al. [12] above 150 keV. Furthermore, although the experimental data of Allison [10] were measured for a molecular hydrogen target, we obtain reasonable agreement with the latter over the whole energy range. Additionally, from Fig. 7 we can learn about the composition of the beam passing through the target. Firstly, above 200 keV projectile energy the beam is comprised almost entirely of protons. As the projectile energy falls the proportion of hydrogen begins to rise, reaching 50% of the beam composition at 50 keV. Be-
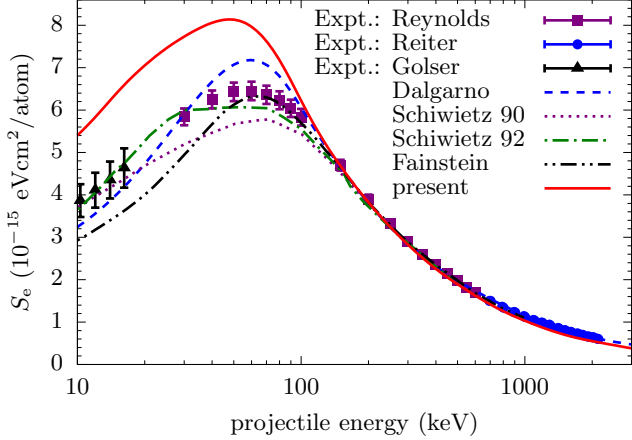
FIG. 8. Total electronic stopping cross section for protons passing through hydrogen. The present results have been obtained using the two-centre CCC method for the positive charge-state contribution and the CCC+B2e (see text for details) method for the neutral charge-state contribution. Also shown are the theoretical calculations of Dalgarno and Griffing [8], Schiwietz [9], Schiwietz and Grande [11], and Fainstein *et al.* [12]. The experimental data of Reynolds *et al.* [5], Reiter *et al.* [6], and Golser and Semrad [7] for protons passing through molecular hydrogen are shown as well.
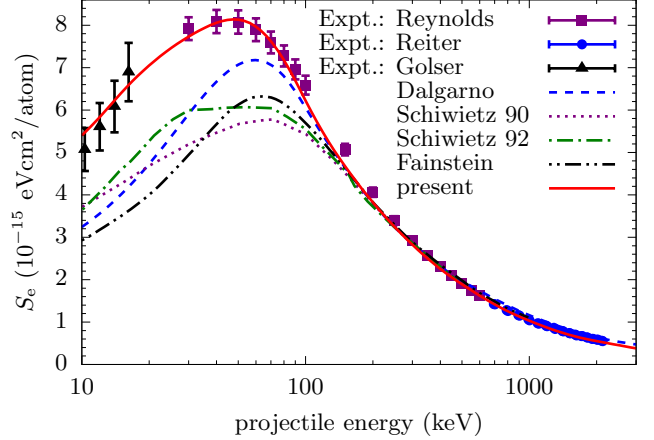

FIG. 9. Total electronic stopping cross section for protons passing through hydrogen. Our present calculations are shown alongside the calculations of Dalgarno and Griffing [8], Schiwietz [9], Schiwietz and Grande [11], and Fainstein *et al.* [12]. Also shown are the experimental data of Reynolds *et al.* [5], Reiter *et al.* [6], and Golser and Semrad [7] for a molecular hydrogen target scaled by the ratio between the atomic- and molecular-hydrogen total ionisation cross sections to provide an estimate of experimental data for an atomic target (see text for details).

low 50 keV hydrogen atoms make up the majority of the beam, reaching 90% of the beam composition at 10 keV.

In Fig. 8 we present our results for the total electronic stopping cross section for protons passing through hydrogen together with the theoretical calculations of Dalgarno and Griffing [8], Schiwietz [9], Schiwietz and Grande [11], and Fainstein *et al.* [12]. Also shown are the experimental results of Reynolds *et al.* [5], Reiter *et al.* [6], and Golser and Semrad [7] for protons passing through molecular hydrogen divided by two, i.e. the results are given per atom as originally presented. Good agreement with the calculations of Dalgarno and Griffing [8] is seen above 100 keV projectile energy, while agreement with the calculations of Schiwietz [9], Schiwietz and Grande [11], and Fainstein *et al.* [12] is obtained above 125 keV. Furthermore, there is good agreement with the experimental data above 150 keV. This demonstrates that the Bragg additivity rule, according to which H_2 is an aggregate of two independent hydrogen atoms, is acceptable above the aforementioned projectile energy. On the other hand, our calculations are significantly above other theoretical estimates and the H_2 experimental data below 100 keV. This fact will be discussed in more detail below. Noticeably, in this region there are substantial deviations between all theoretical approaches. These deviations cannot be attributed to either the positive or neutral charge-state contributions, since there are large deviations between theories in both cases, as seen in Figs. 1 and 3. We can, however, emphasise that our calculations for the positive charge-state contribution are the most sophisticated and accurate as we employ a large two-centre ex-

pansion of the scattering wave function, which explicitly includes electron-capture channels. Furthermore, for the neutral charge-state contribution our approach produces the most accurate projectile total electron-loss cross section.

We conclude by discussing our calculations for atomic hydrogen in comparison to the experimental measurements for molecular hydrogen below 100 keV projectile energy. As can be seen in Fig. 8 there is a significant difference between the two results. The reason for the discrepancy is that Bragg's additivity rule is not valid in this region and, hence, the stopping cross for protons passing through atomic hydrogen can not be represented as a half of the stopping cross section for protons passing through molecular hydrogen. This fact was also demonstrated in our earlier work [18], where a significant difference between the calculated antiproton-atomic hydrogen and antiproton-molecular hydrogen stopping cross sections below the maximum was also observed. Therefore, although some earlier theoretical calculations for atomic hydrogen showed good agreement with experimental data for molecular hydrogen divided by two and the authors claimed this to be a positive aspect of their approach, we emphasise that agreement between the two should not be expected. To further support this statement we can estimate how should experimental data for the proton-atomic hydrogen stopping cross section look like based on the proton-molecular hydrogen stopping cross section data. To this end we scale the proton-H_2 stopping cross section data of Reynolds *et al.* [5], Reiter *et al.* [6], and Golser and Semrad [7] by the ratio between the proton-

hydrogen and proton-H_2 total ionisation cross sections. Ionisation is a dominant energy-loss process and therefore the ratio between the atomic- and molecular-hydrogen ionisation cross sections can provide a reasonable estimate of the ratio between the atomic- and molecular-hydrogen stopping cross sections.

For the ratio between the atomic- and molecular-hydrogen total ionisation cross sections we use the experimental result of Shah and Gilbody [31]. These authors give the ratio from 38 keV to 1.5 MeV. At 1.5 MeV the ratio has plateaued and therefore above this the ratio is taken to be constant. Below 38 keV we calculate the ratio based on the measurements of Shah *et al.* [32] for the atomic target and the measurements of Afrosimov *et al.* [33] for the molecular target. In Fig. 9 we present the same theoretical calculations for the proton-hydrogen total electronic stopping cross section from Fig. 8 alongside the scaled experimental data of Reynolds *et al.* [5], Reiter *et al.* [6], and Golser and Semrad [7]. With the aforementioned scaling of experimental data we obtain excellent agreement over the whole energy range.

IV.   CONCLUSION

In conclusion, the total stopping cross section for protons passing through hydrogen has been calculated. Due to the possibility of electron capture both the positive and neutral charge states of the projectile were considered. To model proton-hydrogen collisions the two-centre CCC method was used. By comparing the results of our two-centre calculations to other single-centre calculations we conclude that singe-centre approaches cannot produced accurate stopping cross sections at low and intermediate incident energies. Hydrogen-hydrogen collisions are modelled using two methods: the single-centre CCC method was used for the calculation of one-electron processes and the Born approximation was used for the calculation of two-electron processes. From the results of these calculations we conclude that the coupling between channels plays an important role in the calculation of one-electron processes. We also conclude that two-electron processes make a significant contribution to the stopping cross section. An evidence is provided that this hybrid approach to modelling hydrogen-hydrogen collisions to gives reliable results. The calculations for the positive and neutral charge states of the projectile were combined by utilising calculated charge-state fractions to yield the total stopping cross section for protons passing through a medium made of atomic hydrogen. Good agreement with all existing theories is obtained above 125 keV incident energy, however below this there is sig-

nificant deviations between the theoretical calculations. From analysing the results of our calculations and experimental data for molecular hydrogen we conclude that around and below the stopping maximum the stopping cross for protons passing through atomic hydrogen can not be represented as a half of the stopping cross section for protons passing through molecular hydrogen. In addition, although some theoretical calculations for atomic hydrogen have attempted to obtain good agreement with experimental data for molecular hydrogen divided by two, we emphasise that agreement between the two should not be expected.

We conclude by commenting on the approximations used in this work. As we mentioned earlier, we neglected electron exchange in the H-H channels. The spin effects are expected to be small in the energy range between 10 keV and 3 MeV where our method is applied. The approximation is commonly used in the literature. In fact, all the theoretical approaches referenced to here use this approximation. However, at low energies, in particular around 10 keV and below, spin effects become important. Nevertheless, no attempt has been made in the literature to estimate the role of the spin effects in stopping of the proton beam. We also neglected electron transfer in H-H collisions. Nevertheless, we did take into account total electron loss by one of the hydrogen atoms. In other words, electron transfer was not completely ignored but taken it into account implicitly. Simply, our approach cannot differentiate whether the lost electron has been captured by the other atom or not. However, as discussed in Sect. III B, comparison of the total cross section for electron loss in H-H collisions with experiment shown in Fig. 4 indicates that overall electron-loss processes have been modelled sufficiently accurately. Thus, the solution we presented in this work is not complete and there is room for improvement. A possible avenue for improving the current results would be to use an antisymmetrised wave function in the H-H channels to take into account the spin effects. However, this would add another dimension to the extraordinary complexity of the problem.

[1] Dž. Belkić, *Theory of Heavy Ion Collision Physics in Hadron Therapy*, Advances in Quantum Chemistry, Vol. 65 (Elsevier,

Amsterdam, 2014).

[2] S. Bakr, D. Cohen, R. Siegele, S. Incerti, V. Ivanchenko, A. Mantero, A. Rosenfeld, and S. Guatelli, Nucl. Instrum. Methods Phys. Res. B **436**, 285 (2018).

[3] J. W. Wilson, J. Miller, A. Konradi, and F. A. Cucinotta, eds., *Shielding Strategies for Human Space Exploration*, NASA conference publication 3360 (Langley Research Center; Hampton, VA United States, 1997).

[4] C. Bertulani, Phys. Lett. B **585**, 35 (2004).

[5] H. K. Reynolds, D. N. F. Dunbar, W. A. Wenzel, and W. Whaling, Phys. Rev. **92**, 742 (1953).

[6] G. Reiter, N. Kniest, E. Pfaff, and G. Clausnitzer, Nucl. Instrum. Methods Phys. Res. B **44**, 399 (1990).

[7] R. Golser and D. Semrad, Nucl. Instrum. Methods Phys. Res. B **69**, 18 (1992).

[8] A. Dalgarno and G. W. Griffing, Proc. R. Soc. A **232**, 423 (1955).

[9] G. Schiwietz, Phys. Rev. A **42**, 296 (1990).

[10] S. K. Allison, Rev. Mod. Phys. **30**, 1137 (1958).

[11] G. Schiwietz and P. L. Grande, Nucl. Instrum. Methods Phys. Res. B **69**, 10 (1992).

[12] P. D. Fainstein, V. H. Ponce, and A. E. Martinez, Phys. Rev. A **47**, 3055 (1993).

[13] F. Borondo, F. Martin, and M. Yanez, Phys. Rev. A **36**, 3630 (1987).

[14] R. Shingal, B. H. Brandsen, and D. R. Flower, J. Phys. B **22**, 855 (1989).

[15] J. B. Wang, J. P. Hansen, and A. Dubois, Phys. Rev. Lett. **85**, 1638 (2000).

[16] M. E. Riley and A. B. Ritchie, J. Phys. B **33**, 5177 (2000).

[17] J. J. Bailey, A. S. Kadyrov, I. B. Abdurakhmanov, D. V. Fursa, and I. Bray, Phys. Rev. A **92**, 022707 (2015).

[18] J. J. Bailey, A. S. Kadyrov, I. B. Abdurakhmanov, D. V. Fursa, and I. Bray, Phys. Rev. A **92**, 052711 (2015).

[19] J. J. Bailey, A. S. Kadyrov, I. B. Abdurakhmanov, D. V. Fursa, and I. Bray, Phys. Med. **32**, 1827 (2016).

[20] I. B. Abdurakhmanov, A. S. Kadyrov, I. Bray, and A. T. Stelbovics, J. Phys. B **44**, 075204 (2011).

[21] I. B. Abdurakhmanov, A. S. Kadyrov, and I. Bray, Phys. Rev. A **94**, 022703 (2016).

[22] I. B. Abdurakhmanov, A. S. Kadyrov, S. K. Avazbaev, and I. Bray, J. Phys. B **49**, 115203 (2016).

[23] S. K. Avazbaev, A. S. Kadyrov, I. B. Abdurakhmanov, D. V. Fursa, and I. Bray, Phys. Rev. A **93**, 022710 (2016).

[24] I. B. Abdurakhmanov, J. J. Bailey, A. S. Kadyrov, and I. Bray, Phys. Rev. A **97**, 032707 (2018).

[25] J. J. Bailey, A. S. Kadyrov, I. B. Abdurakhmanov, and I. Bray, J. Phys. Conf. Ser. **777**, 012010 (2017).

[26] J. Bailey, *Theory of ion-atom collisions for stopping power calculations*, Ph.D. thesis, Curtin University (2018).

[27] E. Guth and C. J. Mullin, Phys. Rev. **83**, 667 (1951).

[28] I. Bray and A. T. Stelbovics, Phys. Rev. A **46**, 6995 (1992).

[29] A. B. Wittkower, G. Levy, and H. B. Gilbody, Proc. Phys. Soc. **91**, 306 (1967).

[30] G. W. McClure, Phys. Rev. **166**, 22 (1968).

[31] M. B. Shah and H. B. Gilbody, J. Phys. B **15**, 3441 (1982).

[32] M. B. Shah, D. S. Elliott, and H. B. Gilbody, J. Phys. B **20**, 2481 (1987).

[33] V. V. Afrosimov, G. A. Leĭko, Yu. A. Mamaev, and M. N. Panov, Sov. Phys. JETP **29**, 648 (1969).